J Mol Model (2010) 16:1509–1518
DOI 10.1007/s00894-010-0660-5

ORIGINAL PAPER

Electronic structure modeling of dinuclear copper(II)-methacrylic acid complex by density functional theory

Serkan Demir · Zuhal Yolcu · Ömer Andaç · Orhan Büyükgüngör · Turan K. Yazıcılar

Received: 27 October 2009 / Accepted: 9 January 2010 / Published online: 21 February 2010

Abstract A dinuclear centrosymmetric copper(II) complex with the formula $[Cu_2(\mu\text{-maa})_4(maaH)_2]$ has been synthesized and experimentally characterized by IR, electronic spectroscopy, and X-ray single-crystal diffractometry. Starting from experimental X-ray geometry and using antiferromagnetic singlet ground state, gas phase geometry optimization was performed by density functional hybrid (B3LYP) method with 6-31G(d) and LANL2DZ basis sets. Gas-phase vibrational frequencies and single point energy (SPE) calculations have been carried out at the geometry-optimized structure. Molecular electrostatic potential calculated at the optimized geometry and natural bond orbital analysis data have been extracted from SPE output. The gas-phase electronic transitions of the title complex were investigated by the time dependent-density functional theory (TD-DFT) approach with the same theory employing LANL2DZ basis set. Also the calculated UV-Vis based upon TD-DFT results and IR spectra were simulated for comparison with the experimental ones.

Keywords B3LYP · DFT · Dinuclear copper(II) · Excited states · LANL2DZ · Methacrylic acid · TD-DFT

S. Demir (✉) · Z. Yolcu · Ö. Andaç · T. K. Yazıcılar
Faculty of Arts and Sciences, Department of Chemistry,
Ondokuz Mayıs University,
55139 Kurupelit,
Samsun, Turkey
e-mail: serkand@omu.edu.tr

O. Büyükgüngör
Faculty of Arts and Sciences, Department of Physics,
Ondokuz Mayıs University,
55139 Kurupelit,
Samsun, Turkey

Introduction

The accurate prediction of molecular properties of transition metal complexes indispensably requires taking electron correlations into account. Therefore, the use of the methods that include electron correlation effects is essential to obtain more reliable informations in addition to experimental findings. Among these, the most prevalent method by coordination chemists is density functional theory (DFT) with its efficient applicability not only to the calculation of the ground state porperties by its static version but also to that of the excited state properties by its time dependent extension (TD)-DFT. In association with the scope of the current paper, the effcient predictions of molecular geometries, vibrational frequencies and electronic transition energies of transition metal systems by DFT methods with exchange correlation functional are well documented [1–6].

DFT requires low computational demands compared to other correlated *ab initio* methods since their accuracy is more dependent to basis set quality than DFT. Thus, DFT offers a promising tool that may be applied to large molecules as transition metal complexes to which application of wavefunction-based electron correlation methods such as moller plesset (MP) or coupled-cluster (CC) is computationally very expensive [7, 8].

The existence of two or more metallic centers in the same molecule can lead to synergistic effects influencing both the chemical and the physical behavior of the molecule such as magnetic, optical or electronic behavior. For this purpose, the selection or design of the bridging ligands is very important because the bridging ligands not only form the backbones of the oligometallic aggregates but can also act as transmitters of metal-metal communication [9]. Based on these considerations, the bridged

transition metal complexes attract considerable attention due to their simple structural and diverse magnetic properties and also ability to mimic the active site in certain proteins [10].

A great deal of copper(II) dinuclear complexes have been synthesized and their magnetic properties have been thoroughly investigated from both the experimental and theoretical point of view [11–14]. In spite of some theoretical contradictions, DFT approachs that include hybrid functionals, most of all B3LYP, have been commonly used to study magnetic structures owing to their efficiency in revealing good estimations of magnetic couplings and subsequently determining the type of magnetism as consistent with experimental results [15, 16]. However, electronic structure calculations and TD-DFT investigations of relevant complexes with B3LYP have not been studied so widely. In our study, we have synthesized a centrosymmetric dinuclear copper(II) complex of methacrylic acid (MaaH) and particularly focused on investigating structural and spectroscopic properties from a calculative point of view comparing to X-Ray data and other experimental measurements. Methacrylic acid can easily be capable of binding metal centers in a bidentate fashion *via* carboxylate oxygens, and is a very suitable ligand for the synthesis of dimeric copper(II) complexes. In the literature, Wu and co-workers synthesized and investigated the structural and magnetic properties of dinuclear copper(II) complexes of methacrylic acid [17–19]. In this work, the homoleptic complex with the formula $[Cu_2(\mu\text{-}maa)_4(maaH)_2]$ has been synthesized, characterized and studied with DFT-B3LYP method and compared with experimental results.

Computational methodology

All computations reported herein were performed using Gaussian 03W program package [20] under Ci symmetry constrain. Experimental geometry obtained from X-ray data was used for the gas-phase ground state DFT optimization. Gas-phase TD-DFT excited state calculations for estimating electronic transition energies were performed based on the optimized geometry. The ground state geometry of the complex was calculated at the hybrid functional B3LYP level of DFT adding LANL2DZ basis set which includes effective core potential set of Hay and Wadt [21] for heavy Cu atom and 6-31G(d) basis set for non-metal atoms. TD-DFT excited state calculations were carried out with the same method employing LANL2DZ basis set for all atoms. As a general rule in the computations, gas-phase frequency analysis was performed at the ground state optimized geometry with the same level of theory. Two different spin cases, a high spin triplet and a broken symmetry (BS) singlet, are extremely possible in the system owing to expected magnetic interactions between copper(II) centers *via* quadruple-bridge methacrylate ligands. In order to obtain the lowest energy state by DFT/UB3LYP method, the wavefunction was checked and found to be stable for both states. Then, the lowest-energy BS singlet state was achieved by using high spin triplet state optimized geometry as initial guess for the low spin BS calculation. Thereafter, the BS singlet ground state was adopted for the modeling of electronic structure of the title complex. DFT models the single determinant wavefunction of non-interactiong electrons but does not properly define the total square spin operator for antiferromagnetic coupling occurring between triplet and pure singlet states. Therefore, BS solution is required to describe open shell low spin state [22]. Although, the most theoretically sound method is the use of multideterminantal approachs for accurate estimations, computationally high demanding requirement of such a methodology necessitates reducing the number of atoms in the calculation [23]. It was reported that alternatively proposed single determinant BS-DFT approach gave the energy of antiferromagnetic singlet for certain compounds with error cancellation and it was fortuitous in theoretical insight that BS-B3LYP predictions of singlet states of dinuclear antiferromagnetic complexes gave consistent results [22]. The absolute determination of this type of coupling requires the knowledge of the exact exchange-correlation functional. Consequently, regarding our computation facilities, BS singlet ground state energy calculated with B3LYP level was preferred as the lowest energy ground state. The energy difference between triplet and BS states was found to be 0.0289 eV in favor of singlet pairing. In addition, the room temperature magnetic susceptibility measurement drawn attention to an antiferromagnetic interaction between two copper(II) centers.

The calculated UV-Vis absorption spectrum in the 200–800 nm wavelength and IR spectrum of the complex were simulated using the *Swizard* program, 4.5 [24] for the comprasion with experimental spectra.

From full population analysis performed by single point energy (SPE) calculation at the optimized geometry and computing one-electron integrals by attaching 3/33=1 overlay option to the input of the calculation, the percentage molecular orbital contributions (MOCs) from atoms and groups to the related Molecular orbitals (MOs) were calculated using *GaussSum version 2.1.6* software package [25].

Molecular electrostatic potential (MEP) is the potential generated by the charge distribution of a molecule and so the sum of multipole moments of molecule and indicates chemical reactivity-nucleophilic and electrophilic sites indicated by MEP contour maps [26]. The potential V(r) created by the nuclei and electrons of system at any point *r*

in the surrounding space can be calculated from the expression [27]:

$$V(r) = \sum_A \frac{Z_A}{|R_A - r|} - \int \frac{\rho(r')}{|r' - r|} dr' \quad (1)$$

where Z_A is the charge on nucleus A at a distance R_A and $\rho(r)$ the electronic density. V_{min} (most negative value or values) is used to analyze sites for electrophilic attack whereas V_{max} (most positive value or values) are essentially related to nuclear charge and not show the sites for nucleophilic attack. Also, MEP is applicable for analyzing non-covalent interactions [27]. Calculation of MEP and potential-derived point charges have been programmed into Gaussian 03W.

Experimental section

Synthesis of the complex

10.0 mmol of copper metal powder (230 mesh) was added dropwise to the solution of a stoichometric amount of methacrylic acid in ethanol (60 ml) and left stirring for 8 hours at room temperature. The red color suspension of copper metal gradually changed to green solution in a period of time. After 8 hours, 30 ml of hexane was added into solution to provide an appropriate solution media for crystallization and needle crystals suitable for x-ray diffraction obtained after 7 days.

Physical measurements

All the solvents and reactants were obtained from commercial suppliers and used without further purification.

IR spectrum was recorded on a Mattson 1000 FTIR spectrometer in the range of 4000–400 cm^{-1} using KBR pellets. UV-Vis spectrum was measured with a UNICAM UV2 spectrometer in the range of 200–900 nm using DMSO as solvent media.

Single crystal x-ray data were collected using STOE X-AREA diffractometer at 100 K(2) using Mo Kα radiation (λ=0,71073 Å). The structure was solved by direct method [28] and refined with full-matrix least squares method [29]. All non-hydrogen atoms were refined anisotropically. Hydrogens bonded to carbon atoms were positioned geometrically and refined with a riding model with U_{iso} 1.2 times that of attached carbon atoms. The positions of O-H hydrogen was obtained from difference fourier map and refined isotropically.

Results and discussion

Crystal structure

The crystal consists of neutral monomeric units and crystallizes in the monoclinic crystal system with the space group of $P2_1/c$. The structure of the complex consists of isolated units of $[Cu_2(Maa)_4(MaaH)_2]$ as shown in Fig. 1. In this units, a quadruple-bridged type dimer of copper atoms seperated by a distance of 2.5959(5) Å and two equivalent copper(II) ions are coordinated by four bridging bidentate methacrylate ligands forming pedal type structure. The axial positions of the metal ions are coordinated by two methacrylic acid molecules. The angles of the coordination polyhedron surrounding the copper(II) listed in Table 1 suggest that the coordination geometry around copper(II) is

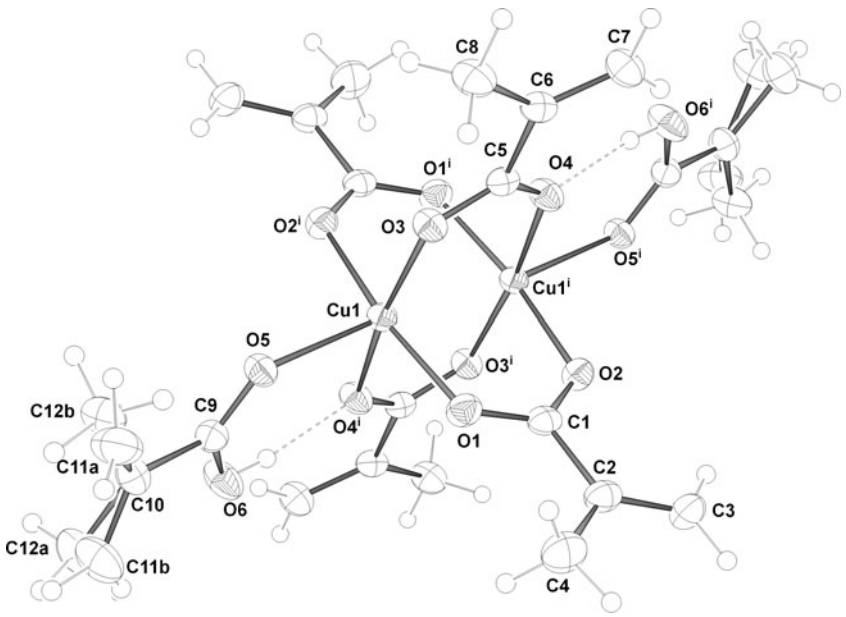

Fig. 1 Molecular view of $[Cu_2(\mu\text{-maa})_4(maaH)_2]$

Table 1 Crystallographic data for $[Cu_2(\mu\text{-maa})_4(maaH)_2]$

Chemical formula	$C_{24}H_{32}Cu_2O_{12}$
Formula weight	639.58
Temperature (K)	100(2)
Wave length (Å)	0.71073
Crystal class	monoclinic
Space group	$P2_1/c$
Unit cell dimensions	
a (Å)	8.7866(6)
b (Å)	19.6646(10)
c (Å)	8.7485(6)
V (Å^3)	1354.89(15)
β (°)	116.321(5)
Z	2
Density calculated (mg/m^3)	1.568
Absorption coefficient (mm^{-1})	1.631
F(000)	660
Crystal size (mm)	0.42 x 0.26 x 0.14
θ range for data collection	2.07–27.09
Reflections collected	20692
Independent reflections	2973 [R(int)=0.0537]
Reflections measured (>2σ)	2387
Absorption correction	Integration
Refinement method	Full-matrix least-squares on F^2
GOF	0.972
final R indces [I>2σ(I)]	R_1=0.0302, wR_2=0.0757
	R_1(all data)=0.0408, wR_2=0.0785
Largest difference peak and hole e (Å^{-3})	0.295 and −0.695

square-based-pyramide with the structural index parameter, Tau, τ=(*Beta-Alpha*)/60=(169.60–169.29)/60=0.01 [30]. In the title compound, the O1-Cu1-O2^i and O3-Cu1-O4^i (i:1-x,-y, 1-z) angles are 169.60(7) and 169.29(6), respectively. Cu(II) ions lies in a centro-symmetric coordination site and center atoms displaced +0,1806(8) Å from the plane composed of O1, O2, O3^i, and O4^i to the axial O5 position. Methyl and vinyl groups of the MaaH in the structure are positionally disordered over two sites (50:50). All MaaH and Maa$^-$ anions are coplanar within the range of deviation of 0,02-0,11 Å. Carboxyl proton of MaaH formed an intramolecular hydrogen bond (D—A=2,603(2)Å and D—H—A=173(4)°) with symmetry related O4 atom and stabilized the structure. Neither conventional nor non-conventional intermolecular hydrogen bond found. Three dimentional structure is formed by wander-waals interactions, Fig. 2.

CCDC 758193 contains the supplementary crystallographic data for this paper. These data can be obtained free of charge *via* www.ccdc.cam.ac.uk/data_request/cif, or by emailing data_request@ccdc.cam.ac.uk, or by contacting The Cambridge Crystallographic Data Centre, 12, Union Road, Cambridge CB2 1EZ, UK; fax: +44 1223 336033.

DFT-B3LYP optimization

For the evaluation of the characters of MOs accurately and the subsequent calculations to be executed meaningfully, gas-phase full optimization of the complex was performed starting from X-ray geometry. Tight SCF convergence applied throughout the calculations implemented in this study to achieve normal termination. Tight optimization was also additionally applied in geometry optimization. The ground state optimized structures and X-ray geometry of the complex were superimposed for visual comparison and shown in Fig. 3. Selected bond lengths and angles compared to the experimental ones are listed in Table 2. The results obtained from the optimization are in reasonable agreement with the values basen on X-ray data. The calculated bond lengths are slightly longer than that of experimental ones with the largest difference of 0.069 Å for $Cu_1 - Cu_1{}^i$ distance as seen in Table 2. This is an expected result for the isolated gas-phase calculation. The calculated geometry reasonably reproduced the X-ray crystal structure and one may say that the increment in bond lengths and angles from solid state to gas phase indirectly reveal the small crystal packing energy. In order to ascertain MOCs and energies, full population analysis was performed. The considered isodensity Frontier occupied and virtual MO surfaces are represented in Fig. 4.

With the examination of MOCs and surfaces, it was determined that all the contributions arise largely from ligand orbitals. Crystal field splitting of center atoms is not identified well as a result of low contributions from d-orbitals. HOMO-2 is localized on almost the whole structure and slightly composed of copper(II) ion with 10% contribution while HOMO (−6.95 eV) is largely composed of isopropenyl moiety of methacrylate with antibonding character. The LUMO (−3.26 eV) mostly originates from metal dx^2-y^2 orbital with a contribution of 64%. The HOMO and HOMO-1 (−6.96 eV) are mostly degenerated only with a difference of 0.012 eV and HOMO-2 (−7.02 eV) is nearly degenerated with the latter two. Also HOMO-3 and HOMO-4 (−7.20 eV,−7,23 eV), LUMO+1 and LUMO+2 (−1.24 eV,−1.24 eV) and LUMO+3 and LUMO+4 (−1.02 eV,−1.03) are well degenerated with each other. The HOMO-LUMO gap is calculated to be −3.66 eV. Owing to BS ground state is considered, both the contributions and surfaces can be given concerning either *alpha* or *beta* orbital as indicated in Fig. 4. The symmetry equivalent of HOMO-*alpha* by the inversion center is HOMO-*beta*.

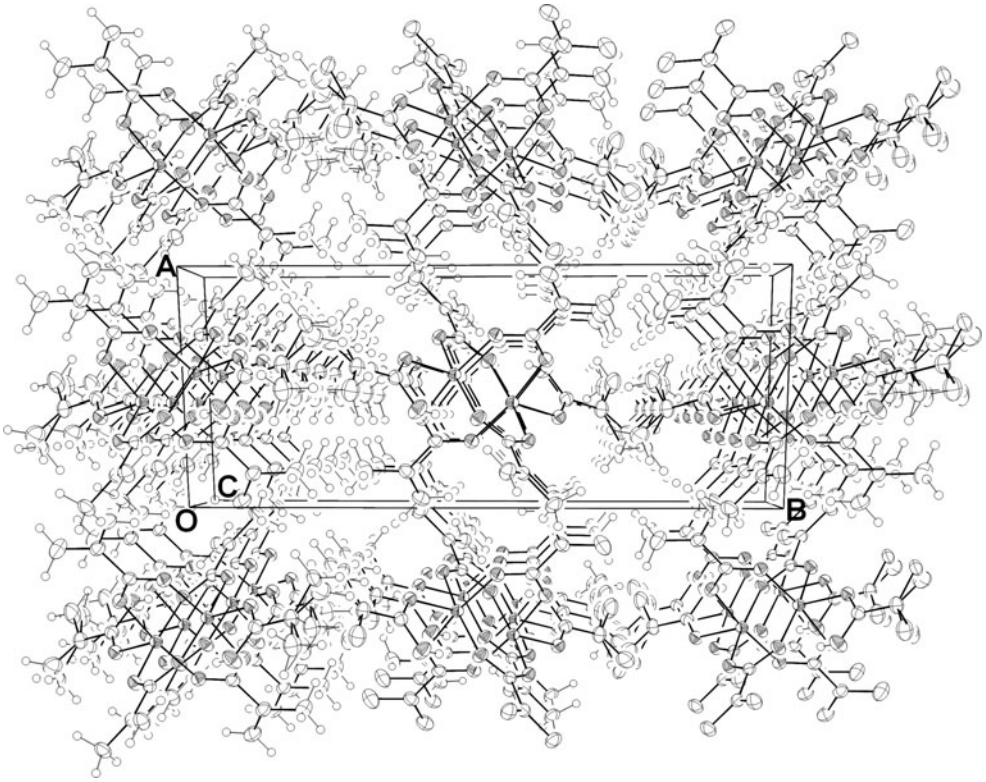

Fig. 2 Crystal structure of $[Cu_2(\mu\text{-maa})_4(maaH)_2]$

Distribution of the electrostatic potential of the ligands was estimated by SPE calculation carried out at the optimized geometry. For the optimization of the ligands, model geometries obtained by Gaussview GUI of Gaussian 03W [31] was used. If the interaction of Lewis donor ligand with Lewis acceptor metal center is normally considered as nucleophilic attack, methacrylate is said to have more nucleophilic behavior as expected than neutral form with a value of V_{min}=−6.39 eV compared to that of neutral form according to the MEP calculation as shown in Fig. 5.

To investigate significant delocalization effects to the coordination environments of the metal centers, the energetic stabilization due to the interactions between donor and acceptor pairs was estimated by second order perturbation theory analysis of the Fock matrix in natural bond orbital (NBO) basis carried out by SPE calculation at the optimized geometry. For each donor NBO (i) and acceptor NBO (j), the stabilization energy associated with delocalization between donor and acceptor is explicitly estimated by Eq. 2 [32]:

$$E = \Delta E_{ij} = q_i \frac{F^2(i,j)}{\varepsilon_j - \varepsilon_i}. \quad (2)$$

Where q_i is the ith donor orbital occupancy, ε_i ; ε_j are diagonal elements (orbital energies) and F(i,j) off diagonal element respectively associated with Fock matrix. Selected interactions that give the strongest stabilization energies are given in Table 3. The interaction energy between Methacrylate oxygens and copper(II) center are also associated with corresponding distance among them. Decrease on the distances between donor oxygens and acceptor center atom is accompanied by the increment in the stabilization energy and concluded by the estimation. For example, the longest O5-Cu1 distance of 2.2261 Å gives the lowest stabilization energy to the structure. The intramolecular H-bond interaction between donor $O4^i$ lone pair and acceptor O6-H6 bond was also revealed by the calculation and constituted a stabilization energy of 11.38 $kcalmol^{-1}$ in the structure as

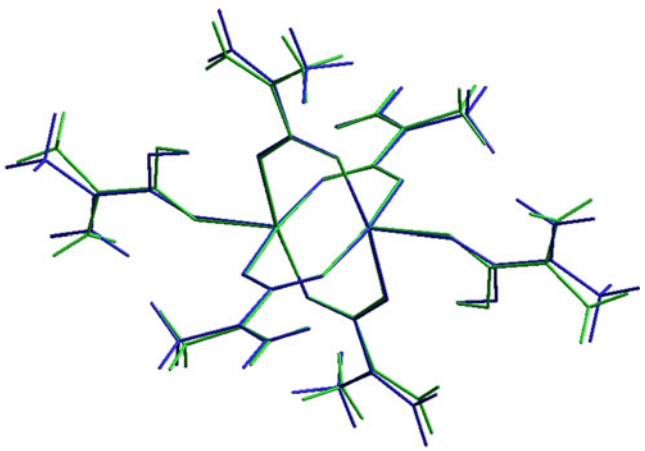

Fig. 3 Superimposition of gas-phase optimized (blue) and experimental (green) geometry of $[Cu_2(\mu\text{-maa})_4(maaH)_2]$

Table 2 Selected Bond lengths and angles of experimental and optimized structures of $[Cu_2(\mu\text{-maa})_4(maaH)_2]$

	Bond lengths (Å)			Bond angles (°)	
	Exp.	Calc.		Exp.	Calc.
Cu1-O1	1.9478(16)	1.9884	O2#1-Cu1-O1	169.60(7)	168.332
Cu1-O2#1	1.9432(15)	1.9758	O1-Cu1-O5	92.67(6)	93.491
Cu1-O3	1.9646(15)	1.9976	O2#1-Cu1-O5	97.63(6)	97.989
Cu1-O4#1	2.0050(14)	2.0486	O3-Cu1-O5	99.80(6)	101.800
Cu1-O5	2.1905(15)	2.2261	O4#1-Cu1-O5	90,89(6)	89.89
Cu1-Cu1#1	2.5959(5)	2.6648	O1-C1-O2	125.2(2)	125.706
O1-C1	1.261(3)	1.2719	O3-C5-O4	123.63(19)	124.510
O2-C1	1.266(3)	1.2704	O5-C9-O6	123.4(2)	123.416
O3-C5	1.254(3)	1.2622	O1-C1-C2	117.0(2)	116.094
O4-C5	1.268(3)	1.2802	O3-Cu1-O4#1	169.29(6)	168.236
O5-C9	1.225(3)	1.2318	O1-Cu1-O4#1	89.23(7)	88.351
O6-C9	1.315(3)	1.3302	O2#1-Cu1-O4#1	89.19(7)	89.582
C1-C2	1.498(3)	1.5053	O1-Cu1-O3	89.55(7)	89.618
C2-C3	1.368(4)	1.3388	O2#1-Cu1-O3	90.10(7)	90.074
C2-C4	1.447(4)	1.5066			
#1:1-x,-y,1-z					

seen in the Table 3. Delocalizations of single π bonds among carboxylate oxygens *via* carbon lone pair unoccupied NBO gives the strongest stabilization energy to the system.

Frequency calculation

In order to facilitate the assignment of the observed peaks, vibrational frequency analysis was performed at the

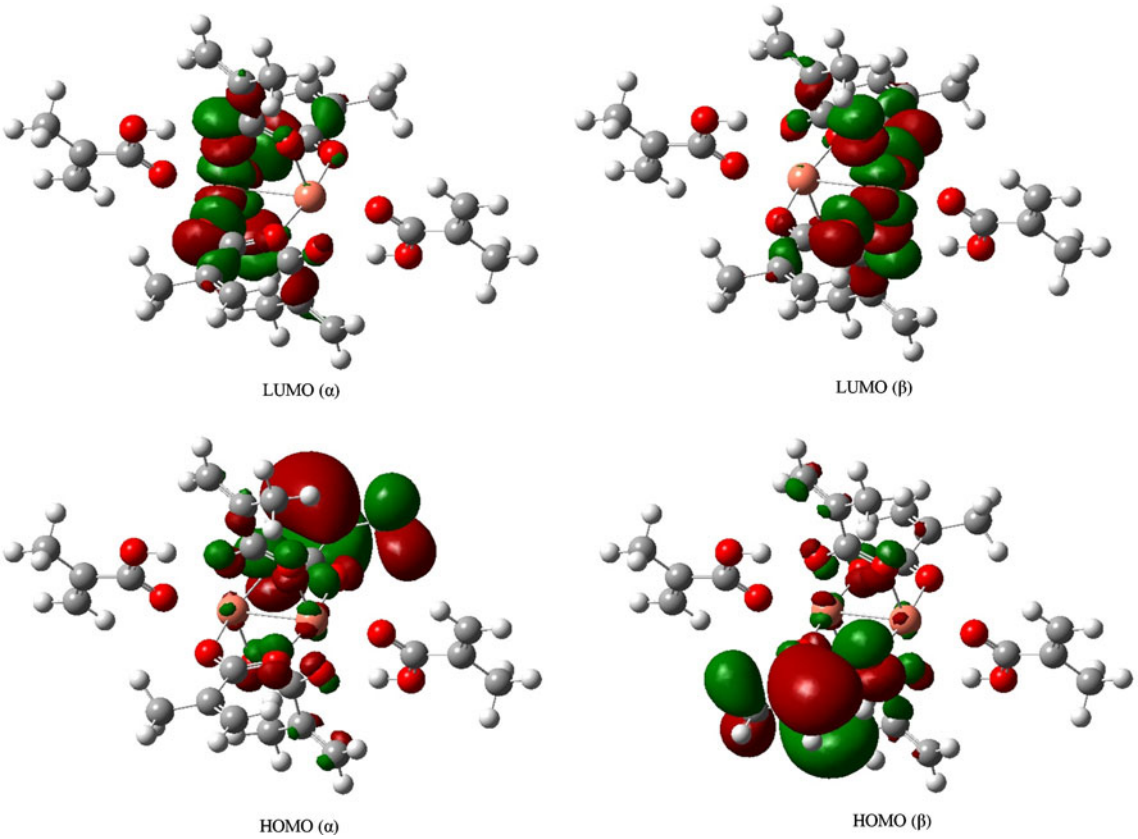

Fig. 4 Frontier molecular orbitals (FMOs) of $Cu_2(\mu\text{-maa})_4(maaH)_2]$

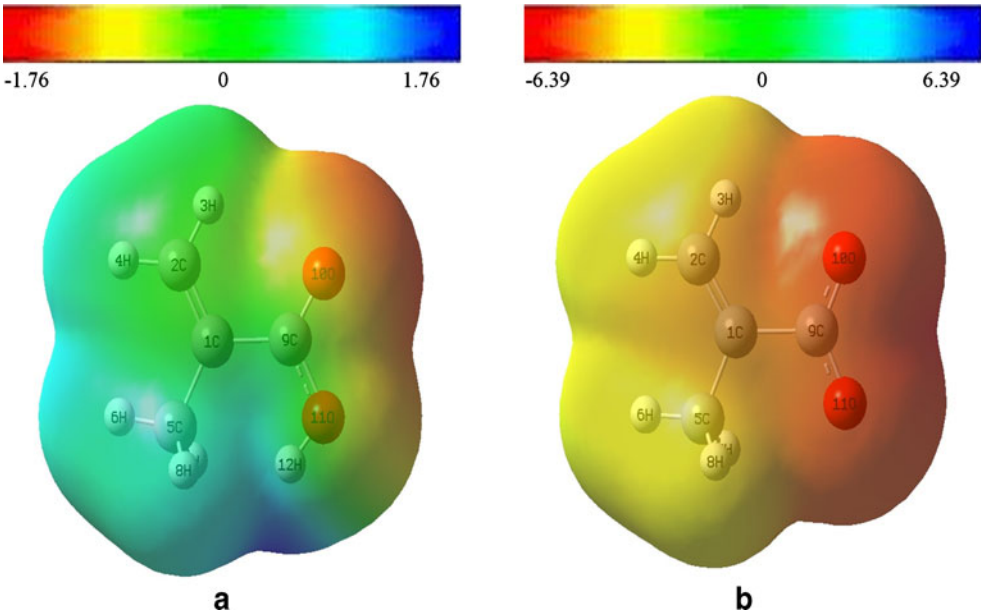

Fig. 5 MEP for the methacrylic acid (**a**) and methacrylate anion (**b**)

optimized geometry with the same level of theory. The calculated and experimental spectral data for the complex are listed in summary in Table 4. Also, Fig. 6 comparatively shows calculated and experimental spectra of the complex. Vibrational band assignments have been made by using Gaussview. In general, vibrational modes obtained from frequency analysis are quite useful to distinguish the observed absorption bands that are difficult to identify due to the overlapping in complicated spectra. Vibrations in Table 4 are scaled by 0.9613 [33] and the values satisfactorily agree with the experimental ones and it is known that small differences arise from gas-phase calculation. Although, the most intense band in the calculated spectra is O-H stretching with an intensity of 2705 km mol^{-1}. The coresponding frequency was underestimated with 5.15% error as a known exception in the DFT/B3LYP level. The second intense band as expected is C=O strecthing with an intensity of 1393 km mol^{-1}. Carboxylate C=O strecthing value at 1587 cm^{-1} is consistent with bond character between C=O double and C-O single bonds [34] and also was reproduced by the calculation. The calculated spectrum is not scaled because it is given for qualitative comparison.

Table 3 Second order perturbation theory analysis of the Fock matrix in NBO basis

Donor	Acceptor	E^2 (kcal/mol)
Cu1(LP)	Cu1′(LP*)	0.55
O1(LP)	Cu1(LP*)	17.42
O3(LP)	Cu1(LP*)	12.13
O5(LP)	Cu1(LP*)	9.36
O2′(LP)	Cu1(LP*)	20.30
O4′(LP)	Cu1(LP*)	14.20
O1-O2(BD)	C1(LP)	223.18
O3-O4(BD)	C5(LP)	214.70
O5-O6(BD)	C9(LP)	213.25
O4′(LP)	O6-H6(BD*)	11.38

LP: a lone pair valence orbital, BD: 2-center bond orbital, BD*: 2-center antibond orbital and LP*: empty valence orbital NBOs

TD-DFT calculations

Starting from DFT/B3LYP optimized geometry, based on BS ground state, TD-DFT excited state calculations were

Table 4 Selected calculated and observed vibrations of $[Cu_2(\mu\text{-maa})_4(maaH)_2]$

Assignment	Exp.	Calc.	Intensity
ν(OH)	3430b	3253	2705
ν_{vin}(CH)	3019w	3047	57
ν(CH)	2960w	2989	53
ν(C=C)	1647 m	1641	179
ν_{as}(COO)	1587vs	1602	1393
$\alpha_{vin}(CH_2)+\delta(CH_3)+\nu$(C=C)	1413 s	1405	110
$\delta(CH_3)+\nu$(C-C)	1374 m	1382	302
β(OH)+ν(C-O)+γ(CH)	1300 m	1283	390
$\gamma_{vin}(CH)+\omega(CH)+\nu_s$(C=O)	1223 m	1220	158
$\gamma_{vin}(CH)+\gamma(CH)+\nu$(C-O)	1203 m	1205	289
ω_{vin}(CH)	946 m	947	58
ω(OH)	826 m	872	200

ν, stretching; γ, rocking; ω, wagging; a, scissoring
δ, twisting; β, bending
vin, vinyl; s, symmetric; as, asymmetric
b=broad; w=weak; m=medium; s=strong vs=very strong;

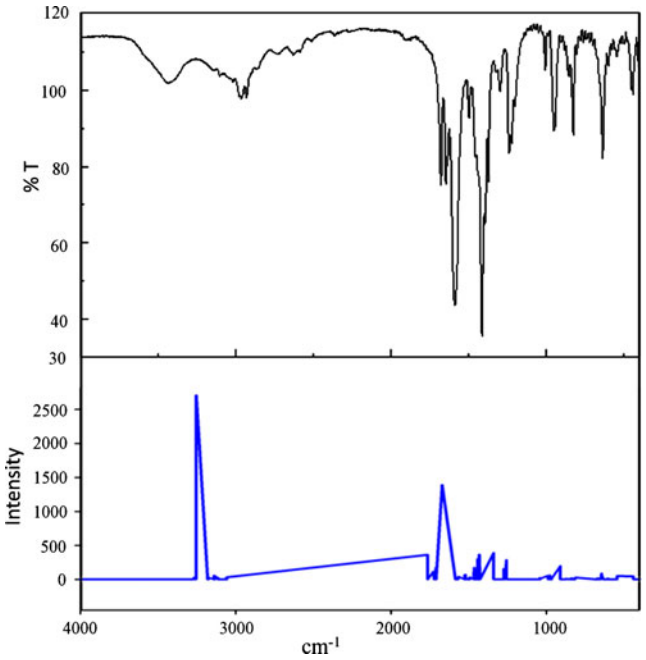

Fig. 6 Experimental (top) and calculated (bottom) IR spectra of $[Cu_2(\mu\text{-maa})_4(maaH)_2]$

Table 5 List of selected transition wavelengths and the major contributions of $[Cu_2(\mu\text{-maa})_4(maaH)_2]$ calculated by TD-DFT method

λ_{max} (Calc.)	λ_{max} (Exp.)	Oscillator strength (f)	Major contribution	eV
678	728	0.0206	H-7→L(32%) H-28→L(20%) H-24→L(13%) H-32→L(7%)	1.83
312	–	0.2298	H-12→L(51%) H-28→L(8%) H-17→L(7%) H-7→L(6%)	3.97
301	–	0.0563	H-16→L(43%) H-18→L(22%) H-17→L(11%)	4.12
286	272	0.1823	H-18→L(56%) H-16→L(12%) H-26→L(9%) H-13→L(6%)	4.33

performed to investigate excitations and for more definite and qualitative description of experimental UV-Vis spectrum. Although a number of methods are available with density functional theory to calculate transition energies, TD-DFT is of particular interest because of giving more reliable results in many transition metal complexes recently studied [35–39] and still a few TD-DFT investigation of spectroscopic properties of dinuclear copper(II) systems have been reported [39, 40]. An effective double-ζ LANL2DZ basis set applied for all atoms in the calculation due to the size of the molecule and large computational demand. Literature survey reveals that LANL2DZ basis set gives consistent results with the experiment for the calculation of vertical excitation energies and can be succesfully applied to tansition metal complexes [40–42]. For the detailed examination of the observed transitions, a series of sucessive TD-DFT calculations were performed. In order to include higher energy ligand-based transitions to the calculation, the first 70 singlet excitations were analyzed. Utilizing data obtained by DFT and TD-DFT calculations, the character of each transition was assigned according to the composition of the occupied and virtual MOs that involves the excitations considered. The establishment of the observed transitions by the calculation were made by utilizing from corresponding oscillator strengths. The percentage contributions to the formation of the bands and oscillator strengths were extracted from output by using Swizard Program. The characters, compositions, and energies of the investigated transitions together with oscillator strengths that are considerably larger than zero were given in Table 5. When the excitations within 200–900 nm range were examined, a transition band at 678 nm with oscillator strength of 0.0206 was estimated in low-energy spectral region. This partially spin-allowed transition is referred to the transition which occured at 728 nm in the experimental spectrum as indicated in Fig. 7, and assigned as d-d transition. A shift by 50 nm mostly may be referred to gas-phase calculation and to strucural differences between optimized and experimental geometries. Optimized geometry was used as the initial guess for the calculation rather than X-ray geometry. Nevertheless, the

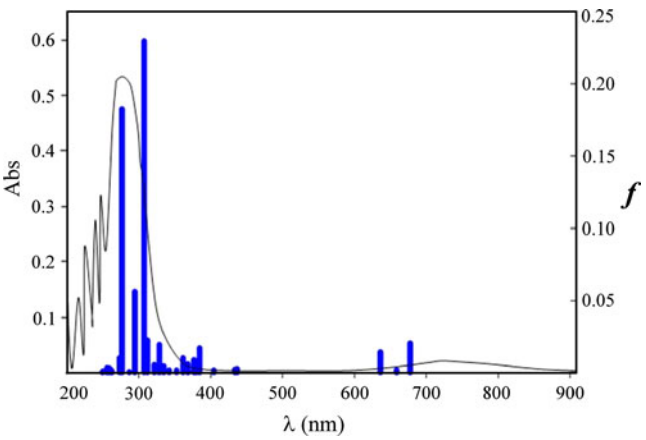

Fig. 7 The observed and calculated UV-Vis spectra of $[Cu_2(\mu\text{-maa})_4(maaH)_2]$

experimental spectrum was reproduced well by the calculated one. In the composition of the band at 678 nm, there is some controversy as to d→d assignement constructed by experimental insight. The main percentages of 32% H-7→L, %20 H-28→L, 13% H-24→L and 7% H-32→L to the composition of the band indicates contributions of ligands to the transition are dominant to that of metal because of the fact that H-7 (7.35 eV) and H-28 (−9.98 eV) are essentially made up of methacrylic acid π orbitals. The corresponding band was determined as π/d→π/d transition by considering largest contributions of %32 and %37 to H-24 (−9.71 eV) and H-32 (−10.18 eV) respectively are from metal d orbitals. The two most intense bands located at 312 nm and 286 nm are made up largely of H-12(−7.90 eV)→L and H-18(−8.45 eV)→L components, respectively. These two bands were also assigned as π→π/d transition and they are probably overlapped with each other in the experimental spectrum. Because approximately half of the most intense vertical excitation coincides with the experimentally observed absorption region as seen in Fig. 7. Owing to relative higher energy of the orbitals above LUMO, contributions from these orbitals to corrsponding transitions are very small related to LUMO and no remarkable transition observed in the region above 250 nm.

Conclusions

A dinuclear $[Cu_2(\mu\text{-maa})_4(maaH)_2]$ complex synthesized and experimentally characterized by X-ray crystallography, IR, and UV-Vis spectroscopy techniques. Density functional B3LYP calculations adopting BS singlet ground state with unrestricted formalism have been carried out to investigate structural and spectroscopic properties as the main scope of this work. Although TD-DFT approach is widely used and successfully applied for transition metal systems, it is not commonly used for dinuclear transition metal systems. So it was applied starting from optimized geometry to determine the assignements of observed electronic excitations in title complex. NBO analysis which is mainly used to gain insight into *inter* or *intra*molecular interaction stabilities has been utilized to investigate bonding interactions within the structure. With the exception of OH strecthing vibration of %5.05 error in frequency calculation and the composition of the absorbtion band at 678 nm in TD-DFT calculations, the obtained results have presented reasonable consistency with the experiment. Other than gas-phase calculation, one can say that the noticable differences between calculated and experimental data arise from small structural differences between optimized and X-ray geometries as well as from the level of theory used. The general trends observed in experimental data have been reproduced by the calculations.

References

1. Chermette H (1998) Coord Chem Rev 178–180:699–721, dftaccuracy
2. Autschbach J (2007) Coord Chem Rev 251:1796–1821, review4
3. Charles W, Bausclicher JR (1995) Chem Phys Lett 246:40–44
4. Neese F (2009) Coord Chem Rev 253:526–563, review3
5. Holland JP, Barnard PJ, Bayly SR, Dilworthy JR, Green JC (2009) Inorg Chim Acta 362:402–406, nickelTDDFT
6. Holland JP, Green JC (2009) J Comput Chem 00:00. DOI:10.1002/jcc.21385) (evaluation_of)
7. Pu-Su Z, Fang-Fang J, Chun-Lei L, Jian Z (2006) Chin J Struct Chem 25:657–662
8. Viruela PM, Viruela R, Orti E, Brédas JL (1997) J Am Chem Soc 119:1360–1369
9. Morawitz T, Bolte M, Lerner HW, Wagner M (2008) Z Anorg Allg Chem 634:1409–1414
10. Sun YM, Wang LL, Wu JS (2008) Transition Met Chem 33:1035–1040
11. Hu ZC, Wei HY, Chen ZD (2004) J Mol Struct THEOCHEM 668:235–242
12. Bencini A, Costes JP, Dahan F, Dupuis A, Garcia-Tojal J, Gatteschi D, Totti F (2004)
13. Noh EAA, Zhang J (2006) Chem Phys 330:82–89
14. Plaul D, Geibig D, Görls H, Plass W (2009) Polyhedron 28:1982–1990
15. Beobide G, Castillo O, García-Couceiro U, García-Terán JP, Luque A, Martínez-Ripll M and Román P (2005) Eur J Inorg Chem 2586–2589
16. Aronica C, Jeanneau E, El Moll H, Luneau D, Gillon B, Goujon A, Cousson A, Carvajal MA, Robert V (2007) Chem Eur J 13:3666–3674
17. Wu B, Lu WM, Zheng XM (2002) J Coord Chem 55:497–503
18. Wu B, Lu WM, Zheng XM (2002) Chin J Chem 20:846–850
19. Wu B, Lu WM, Zheng XM (2003) Transition Metal Chemistry 28:323–325
20. Frisch MJ, Trucks GW, Schlegel HB, Scuseria GE, Robb MA, Cheeseman JR, Montgomery JA Jr, Vreven T, Kudin KN, Burant JC, Millam JM, Iyengar SS, Tomasi J, Barone V, Mennucci B, Cossi M, Scalmani G, Rega N, Petersson GA, Nakatsuji H, Hada M, Ehara M, Toyota K, Fukuda R, Hasegawa J, Ishida M, Nakajima T, Honda Y, Kitao O, Nakai H, Klene M, Li X, Knox JE, Hratchian HP, Cross JB, Adamo C, Jaramillo J, Gomperts R, Stratmann RE, Yazyev O, Austin AJ, Cammi R, Pomelli C, Ochterski JW, Ayala PY, Morokuma K, Voth GA, Salvador P, Dannenberg JJ, Zakrzewski VG, Dapprich S, Daniels AD, Strain MC, Farkas O, Malick DK, Rabuck AD, Raghavachari K, Foresman JB, Ortiz JV, Cui Q, Baboul AG, Clifford S, Cioslowski J, Stefanov BB, Liu G, Liashenko A, Piskorz P, Komaromi I, Martin RL, Fox DJ, Keith T, Al-Laham MA, Peng CY, Nanayakkara A, Challacombe M, Gill PMW, Johnson B, Chen W, Wong WM, Gonzalez C, Pople JA (2003) Gaussian 03W, Version 6.1. Gaussian Inc, Pittsburgh
21. Hay PJ, Wadt WR (1985) J Chem Phys 82:299
22. Moreira IPR, Illas F (2006) Phys Chem Chem Phys 8:1645–1659
23. Ruiz E, Cano J, Alvarez S, Alemany P (1999) J Comput Chem 20:1391–1400
24. Gorelsky SI, SWizard program, Revision 4.5 http://www.sg-chem.net/
25. O'Boyle NM, Tenderholt AL, Langner KM (2007) J Comput Chem 29:839–845
26. Donglai W, Hongtao S, Yuchun Z (2007) J Rare Earths 25:210–214
27. Politzer P, Murray JS, Concha MC (2002) Int J Quantum Chem 88:19–27

28. Altomare A, Burla MC, Camalli M, Cascarano GL, Giacovazzo C, Guagliardi A, Moliterni AGG, Polidori G, Spagna R, Sir97 (1999) J Appl Cryst 32:115–119
29. Sheldrick GM, Shelxl-97 (1997) University of Göttingen, Germany
30. Addison AW, Rao TN, Reedijk J, Van Rijn J, Verschoor GC (1984) J Chem Soc Dalton Trans 1349
31. Frisch A, Dennington R II, Keith T, Millam J, Nielsen AB, Holder AJ, Hiscocks J (2007) GaussView reference, Version 4.0. Gaussian Inc, Pittsburgh
32. Ghiasi R, Monnajemi M (2006) J Korean Chem Soc 50:281–291
33. Curtiss LA, Raghavachari K, Redfern PC, Pople JA (1997) Chem Phys Lett 270:416–426
34. Field LD, Sternhell S, Kalman JR (2007) Organic structures from spectra, 4th edn
35. Nemykin VN, Olsen JG, Perera E, Basu P (2006) Inorg Chem 45:3557–3568
36. Nemykin VN, Makarova EA, Grosland JO, Hadt GR, Koposov AY (2007) Inorg Chem 46:9591–9601
37. Donzello MP, Ercolani C, Kadish KM, Ricciardi G, Rosa A, Stuzhin PA (2007) Inorg Chem 46:4145–4157
38. Di Censo D, Fantacci S, De Angelis F, Klein C, Evans N, Kalyanasundaram K, Bolink HJ, Gr tzel M, Nazeeruddin MK (2008) Inorg Chem 47:980–989
39. Basu C, Biswas S, Chattopadhyay AK, Stoeckli-Evans H, Mukherjee S (2008) Eur J Inorg Chem 4927–4935
40. Gahungu G, Zhang J (2005) Chem Phys Lett 410:302–306
41. Wakamatsu K, Nishimoto K, Shibahara T (2000) Inorg Chem Commun 3:677–679
42. Machura B, Świtlicka A, Kruszynski R, Kusz J, Penczek R (2008) Polyhedron 27:2513–2518